the extrapolated low- and high-temperature lines. Straight lines are drawn through the points in the high- and low-temperature regions. The point where the midpoint between these two lines intersects the curved line connecting the data points in the region of the critical temperature is determined. This point in the plot of band gap energy vs. temperature is defined as the phase-transition temperature. The midpoint temperatures are 68 °C for the copper compound and 47 °C for the silver compound.

The DSC plots exhibit a sharp exotherm at 68 °C for the copper compound and at 50 °C for the silver compound. The exotherms are very sharp with a width at half-height of 3 deg. The phase-transition temperatures determined by DSC are in excellent agreement with those determined from the band gap measurements.

The sensitivity of the electronic transition energy to subtle changes in the crystal lattice is evident in Figure 4. The nonzero slope in the linear regions is caused by the expansion of the lattice with increasing temperature and the subtle changes in the positions of the ions are caused by increased populations of anharmonic vibrational modes. The linear decrease in energy with increasing temperature is consistent with the simple one-electron spectroscopic model discussed above. As the lattice expands, the antibonding mercury s orbitals decrease in energy while the energies of the nonbonding iodide p orbitals change only slightly, giving rise to a decrease in the transition energy.

The mechanism of the phase transition has been explained by LeDuc, et al.[18] The transition is first order. The large mercury ions act as a valve prohibiting mobile silver (or copper) ions from disordering by blocking the conduction paths. When the thermal energy becomes high enough to allow the mercury ions to surmount their potential barriers, a large number of silver (or copper) ion carriers exist with high enough thermal energy to enter the vacant sites. Disordering then occurs rapidly. The optical data support this explanation. The nonlinear changes measured by this sensitive technique only occur over a small temperature range near the transition temperature.

Acknowledgment. Funds for this work were provided by the Naval Facilities Engineering Command, Alexandria, VA, and the Office of Naval Research, Arlington, VA. We wish to thank Jay Lee (a summer intern at NCEL) and the analytical chemistry groups at NWC China Lake and at NCEL, Port Hueneme, CA, for assistance in the syntheses and DSC measurements.

Contribution from the Department of Chemistry, Memorial University of Newfoundland, St. John's, Newfoundland, Canada A1B 3X7, Department of Inorganic Chemistry, Indian Association for the Cultivation of Science, Calcutta 100032, India, and Division of Chemistry, National Research Council, Ottawa, Ontario, Canada K1A 0R6

Synthesis, Structure, and Electrochemistry of a Novel Macrocyclic Dicopper(II) Complex. Four One-Electron-Transfer Steps Producing Binuclear Copper(III) and Copper(I) Species and Mixed-Valence-State Species

Sanat K. Mandal,[1a] Laurence K. Thompson,*[1a] Kamalaksha Nag,*[1b] Jean-Pierre Charland,[1c] and Eric J. Gabe†[1c]

Received December 5, 1986

The antiferromagnetically coupled macrocyclic binuclear copper(II) complex $[Cu_2L1(ClO_4)_2]$ (1), involving the saturated ligand H_2L1 ($C_{24}H_{36}N_4O_2$), derived by template condensation of 4-methyl-2,6-diformylphenol with 1,3-diaminopropane, followed by borohydride reduction, exhibits cyclic voltammetry involving two one-electron oxidation steps ($E_{1/2}$ = 1.21, 1.41 V; Pt/CH_3CN) and two one-electron reduction steps ($E_{1/2}$ = -0.76, -0.90 V; GC/Me_2SO) with the formation of Cu(III)-Cu(III), Cu(II)-Cu(I), and mixed-oxidation-state species. Complex 1 has been characterized by single-crystal X-ray diffraction and compared electrochemically with analogous complexes involving related ligands with half-saturation and full unsaturation at the azomethine centers. The degree of ligand saturation has a dramatic effect on both oxidation and reduction potentials. Complex 1 crystallizes in the orthorhombic system, space group *Fddd*, with a = 16.985 (2) Å, b = 17.180 (3) Å, c = 20.558 (4) Å, Z = 8. The two copper(II) centers have distorted N_2O_2 in-plane donor sets, involving two phenoxide bridges, with a copper-copper separation of 2.993 (2) Å. Long axial interactions (Cu-O = 2.821 (3) Å) with bridging bidentate perchlorates complete the distorted copper octahedra.

Introduction

The development of the chemistry of macrocyclic binuclear complexes has been stimulated by a desire to "mimic" the active sites of metallobiomolecules,[2] to evaluate appropriate systems for binding and activation of small molecules,[3] and to investigate the mutual influence of two metal centers on the electronic, magnetic, and redox properties of such systems.[3,4] To this end, metal complexes of the ligand H_2L3 (Figure 1), and its derivatives, have been the focus of extensive studies.[4-11] We have been interested to know how stereochemistry, reactivity, and redox behavior of binuclear copper complexes of this sort are affected by gradual reduction of the azomethine linkages of H_2L3 (H_2L2, H_2L1; Figure 1). The synthesis and electrochemistry of the dicopper(II) complexes of H_2L2, and its analogues, at negative potentials (reduction steps only), have been reported recently.[12] We now report the preparation, characterization, structure, and electrochemistry of the phenoxo-bridged dicopper(II) complex $[Cu_2L1(ClO_4)_2]$ (1) and an electrochemical comparison of this

* To whom correspondence should be addressed.
† NRCC Contribution No. 27341.

(1) (a) Memorial University. (b) Indian Association for the Cultivation of Science. (c) National Research Council.
(2) See, for example: (a) Coughlin, P. K.; Lippard, S. J. *J. Am. Chem. Soc.* **1984**, *106*, 2328. (b) Agnus, Y.; Louis, R.; Gisselbrecht, J.-P.; Weiss, R. *J. Am. Chem. Soc.* **1984**, *106*, 93.
(3) (a) Lehn, J. M. *Pure Appl. Chem.* **1980**, *52*, 2441. (b) Nelson, S. M. *Pure Appl. Chem.* **1980**, *52*, 2461. (c) Fenton, D. E.; Casellato, V.; Vigato, P. A.; Vidali, M. *Inorg. Chim. Acta* **1982**, *62*, 57.
(4) Groh, S. E. *Isr. J. Chem.* **1976-1977**, *15*, 277.
(5) Pilkington, N. H.; Robson, R. *Aust. J. Chem.* **1970**, *23*, 2225.
(6) Okawa, H.; Kida, S. *Bull. Chem. Soc. Jpn.* **1972**, *45*, 1759.
(7) (a) Hoskins, B. F.; Williams, G. A. *Aust. J. Chem.* **1975**, *28*, 2607. (b) Hoskins, B. F.; McLeod, N. J.; Schaap, H. A. *Aust. J. Chem.* **1976**, *29*, 515.
(8) Addison, A. W. *Inorg. Nucl. Chem. Lett.* **1976**, *12*, 899.
(9) (a) Gagné, R. R.; Koval, C. A.; Smith, T. J.; Cimolino, M. C. *J. Am. Chem. Soc.* **1979**, *101*, 4571. (b) Gagné, R. R.; Spiro, C. L.; Smith, T. J.; Hamann, C. A.; Thies, W. R.; Shiemke, A. K. *J. Am. Chem. Soc.* **1981**, *103*, 4073. (c) Spiro, C. L.; Lambert, S. E.; Smith, T. J.; Duesler, E. N.; Gagné, R. R.; Hendrickson, D. N. *Inorg. Chem.* **1981**, *20*, 1229.

0020-1669/87/1326-1391$01.50/0

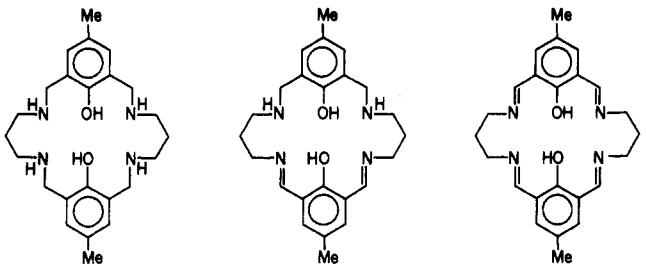

Figure 1. Ligands H_2L1, H_2L2, and H_2L3.

Table I. Crystal Data for $[Cu_2L1(ClO_4)_2]$ (1)

formula	$Cu_2C_{24}H_{34}N_4O_{10}Cl_2$	temp for data collection, K	295
M_r	736.29		
space group	*Fddd*	radiation, Å	λ(Mo Kα) = 0.709 30
a, Å	16.9855 (21)		
b, Å	17.180 (3)	μ, mm^{-1}	1.66
c, Å	20.558 (4)	no. of unique data	1047
V, Å^3	5999.0	no. of unique data with $I_{net} >$ $2.5\sigma(I_{net})$	698
Z	8		
ρ_{calcd}, g cm^{-3}	1.631	*R*, R_w	0.041, 0.017

complex with $[Cu_2L2](ClO_4)_2 \cdot 2H_2O$ (2) and $[Cu_2L3](ClO_4)_2 \cdot 2H_2O$ (3) in two different solvents. The remarkable feature of the complex $[Cu_2L1(ClO_4)_2]$ is that it undergoes four sequential one-electron transfers to generate dicopper species with oxidation states varying from +1 to +3, which, to our knowledge, is unprecedented in coupled systems of this sort.

Experimental Section

Physical Measurements. The electrochemical measurements were performed at room temperature in dimethyl sulfoxide (Me_2SO) (dried over molecular sieves) and acetonitrile (spectroscopic grade dried over molecular sieves) under O_2-free conditions by using a BAS CV27 voltammograph and a Houston Omnigraph 2000 X-Y recorder. A three-electrode system was used (cyclic voltammetry), in which the working electrode was either glassy carbon (reduction in Me_2SO) or platinum (oxidation in acetonitrile), the counter electrode platinum, and the reference electrode a standard calomel (SCE) electrode. For coulometry measurements a three-electrode system was employed, consisting of a platinum-mesh-flag working electrode, a platinum-mesh counter electrode, and a silver rod as the reference electrode. The supporting electrolyte was tetraethylammonium perchlorate (TEAP) (0.1 M), and all solutions were 10^{-3}–10^{-4} M in complex. EPR spectra were run at room temperature with a Varian E-4 spectrometer on electrochemically oxidized and reduced solution species, which were generated in an inert-atmosphere drybox (Vacuum Atmospheres) by using Princeton Applied Research instrumentation and then transferred to EPR tubes (York University). Infrared spectra were obtained with a Perkin-Elmer 283 spectrometer and UV/vis spectra with a Cary 17 spectrometer.

Crystal Structure Determination. X-ray Study of $[Cu_2L1(ClO_4)_2]$ (1). Crystals of 1 are deep blue. The diffraction intensities of an approximately 0.20 × 0.20 × 0.20 mm crystal were collected by using a Nonius diffractometer, graphite-monochromatized Mo Kα radiation, and the omega scan mode to $2\theta_{max} = 45°$. A total of 3492 reflections were measured, of which 1047 were unique and 698 were considered significant with $I_{net} > 2.5\sigma(I_{net})$. Lorentz and polarization factors were applied, but no correction was made for absorption. The cell parameters (Table I) were obtained by the least-squares refinement of the setting angles of 25 reflections with $2\theta = 40$–$45°$ (λ(Mo Kα) = 0.709 30 Å).

Solution and Refinement of the Structure of 1. The structure was solved by direct and difference Fourier methods using the NRCVAX crystal structure programs[13] and refined by full matrix least-squares methods to final residuals of *R* and R_w of 0.041 and 0.017, respectively [$R = \sum(|F_o| - |F_c|)/\sum(|F_o|)$; $R_w = \sum w(|F_o| - |F_c|)^2/\sum w(|F_o|)^2$]. The final difference map had no peaks greater than 0.46 e Å^{-3}. The positions of the hydrogen atoms were all located from difference maps. Scattering factors for neutral species were taken from ref 14. A summary of crystal data is given in Table I, and atomic coordinates are given in Table II. Anisotropic thermal parameters (Table SI) and a listing of structure factors (Table SII) are included as supplementary material.

Table II. Final Atomic Positional Parameters and Equivalent Isotropic Debye–Waller Temperature Factors (Esd's) for $[Cu_2L1(ClO_4)_2]$ (1)

atom	*x*	*y*	*z*	B_{iso}, Å^2
Cu(1)	0.37500 (0)	0.37500 (0)	0.30222 (4)	4.93 (5)
Cl(1)	0.33124 (13)	0.62500 (0)	0.12500 (0)	5.74 (12)
O(1)	0.37840 (28)	0.56961 (23)	0.09829 (20)	14.5 (4)
O(2)	0.28509 (20)	0.59110 (18)	0.17475 (16)	7.9 (2)
O(3)	0.37500 (0)	0.44455 (22)	0.37500 (0)	4.5 (2)
N(1)	0.3943 (3)	0.4593 (3)	0.2381 (3)	5.2 (3)
C(1)	0.3750 (0)	0.5222 (4)	0.3750 (0)	4.6 (4)
C(2)	0.4065 (3)	0.5632 (3)	0.3225 (3)	5.1 (3)
C(3)	0.4044 (4)	0.6454 (3)	0.3231 (3)	6.3 (4)
C(4)	0.3750 (0)	0.6863 (5)	0.3750 (0)	7.1 (6)
C(5)	0.3750 (0)	0.7746 (6)	0.3750 (0)	9.2 (11)
C(6)	0.4446 (4)	0.5220 (4)	0.2674 (3)	5.9 (4)
C(7)	0.4316 (4)	0.4243 (4)	0.1802 (4)	6.3 (4)
C(8)	0.3750 (0)	0.3750 (0)	0.1416 (5)	7.0 (7)
H(1)	0.3509 (28)	0.4772 (27)	0.2234 (24)	6.9 (19)
H(3)	0.4277 (23)	0.6741 (22)	0.2838 (18)	5.6 (14)
H(8)	0.4061 (24)	0.3432 (23)	0.1122 (21)	6.1 (16)
H(51)	0.3753 (72)	0.7924 (41)	0.3277 (26)	0.9 (17)
H(52)	0.4175 (54)	0.8054 (43)	0.3897 (58)	3.2 (23)
H(53)	0.3106 (46)	0.7930 (47)	0.4085 (45)	3.7 (22)
H(61)	0.4938 (21)	0.4930 (19)	0.2776 (18)	4.1 (12)
H(62)	0.4636 (24)	0.5544 (24)	0.2273 (21)	6.9 (14)
H(71)	0.4518 (22)	0.4685 (23)	0.1501 (19)	6.1 (14)
H(72)	0.4748 (23)	0.3940 (25)	0.1979 (20)	6.7 (15)

Table III. Interatomic Distances (Å) and Angles (deg) Relevant to the Copper Coordination Spheres in $[Cu_2L1(ClO_4)_2]$ (1)

Cu(1)–N(1)	1.986 (5)	Cu(1)–O(2)	2.821 (3)
Cu(1)–O(3)	1.915 (3)	Cu(1)–Cu(1)A	2.993 (2)
Cu(1)–O(3)–Cu(1)A	102.8 (2)	O(2)C–Cu(1)–N(1)A	96.9 (2)
O(2)C–Cu(1)–O(2)	160.7 (1)	O(3)–Cu(1)–O(3)A	77.2 (1)
O(2)C–Cu(1)–O(3)	89.9 (1)	O(3)–Cu(1)–N(1)	93.6 (2)
O(2)C–Cu(1)–O(3)A	74.9 (1)	O(3)–Cu(1)–N(1)A	166.9 (2)
O(2)C–Cu(1)–N(1)	95.9 (2)	N(1)–Cu(1)–N(1)A	96.9 (2)

Synthesis of Compounds. H_2L1. A mixture of $Pb(OAc)_2 \cdot 3H_2O$ (5.7 g, 15 mmol) and $Pb(NO_3)_2$ (5.0 g, 15 mmol) dissolved in hot DMF (20 mL) was added to a boiling methanol solution (50 mL) of 4-methyl-2,6-diformylphenol[15] (4.9 g, 30 mmol) followed immediately by 1,3-diaminopropane (2.2 g, 30 mmol) dissolved in methanol (20 mL), and the resulting mixture was refluxed for 8 h. An orange-yellow crystalline product formed (analytical data indicate this compound to be $Pb_2L(NO_3)_2 \cdot 4H_2O$), which was collected by filtration, washed with methanol and chloroform, and dried in air (yield 80%). $Pb_2L(NO_3)_2 \cdot 4H_2O$ (7.3 g, 7.2 mmol) was ground to a fine powder and suspended in methanol (200 mL). A solution of $NaBH_4$ (2.7 g, 70 mmol) in water (10 mL) was added to the stirred suspension over a period of 30 min at 25 °C and the stirring continued for 2 h, during which time a colorless solution formed. The solution was filtered and the filtrate reduced in volume to 50 mL, diluted with water (400 mL), and acidified with cold H_2SO_4 (8 M). The $PbSO_4$ that formed was removed by filtration and washed several times with cold water. The combined filtrate was treated with ammonia in an ice bath until the pH reached ~10 and then extracted with $CHCl_3$ (4 × 50 mL). The $CHCl_3$ solution was dried with anhydrous Na_2SO_4 and evaporated to dryness. The residue was extracted with boiling petroleum ether (80–100 °C), which on slow evaporation gave colorless cubic crystals (yield 61%) (mp 125 °C). Anal. Calcd for $C_{24}H_{36}N_4O_2$: C, 69.90; H, 8.74; N, 13.59. Found: C, 69.75; H, 8.68; N, 13.47. ^{1}H NMR ($CDCl_3/Me_4Si$): δ 1.86 (q, 4 H, $CH_2CH_2CH_2$), 2.18 (s, 6 H, Me), 2.58 (t, 8 H, $CH_2CH_2CH_2$), 3.83 (s, 8 H, $ArCH_2$), 5.1 (br, 6 H, NH and OH), 6.74 (s, 4 H, Ph).

(10) (a) Long, R. C.; Hendrickson, D. N. *J. Am. Chem. Soc.* **1983**, *105*, 1513. (b) Lambert, S. L.; Hendrickson, D. N. *Inorg. Chem.* **1979**, *18*, 2683.
(11) Mandal, S. K.; Nag, K. *J. Chem. Soc., Dalton Trans.* **1983**, 2429.
(12) (a) Mandal, S. K.; Nag, K. *J. Chem. Soc., Dalton Trans.* **1984**, 2141. (b) Mandal, S. K.; Adhikary, B.; Nag, K. *J. Chem. Soc., Dalton Trans.* **1986**, 1175.
(13) Gabe, E. J.; Lee, F. L.; Le Page, Y. In *Crystallographic Computing III*; Sheldrick, G. M., Kruger, C., Goddard, R., Eds.; Clarendon: Oxford, England, 1985; p 167.
(14) *International Tables for X-ray Crystallography*; Kynoch: Birmingham, England, 1974; Vol. IV, Table 2.2B, p 99.
(15) Ullman, F.; Brittner, K. *Chem. Ber.* **1909**, *42*, 2539.

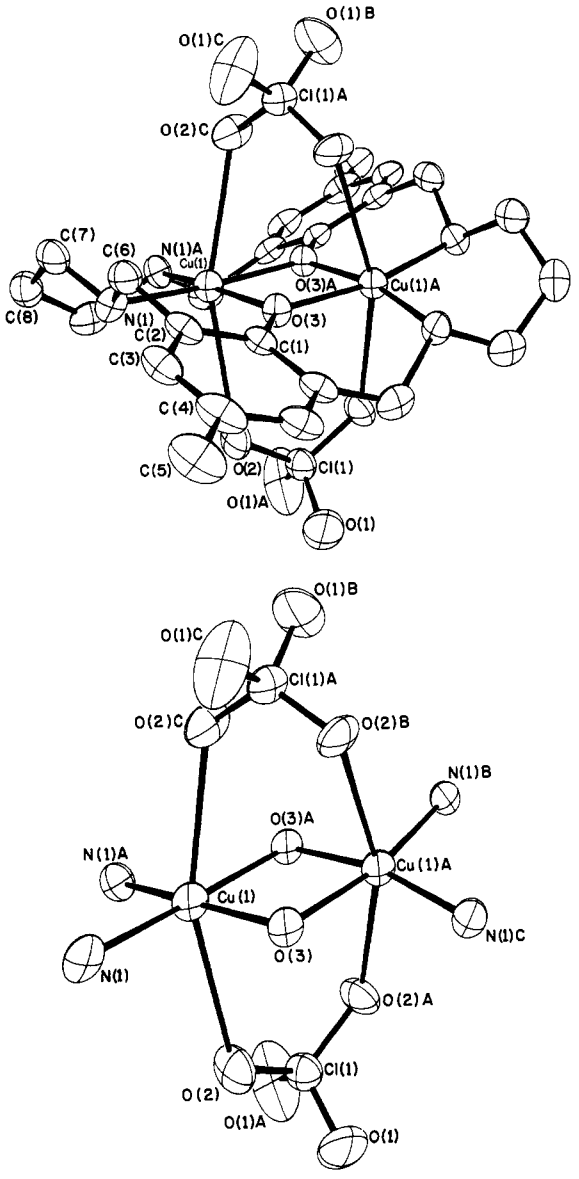

Figure 2. Structure of $[Cu_2L1(ClO_4)_2]$ (**1**) showing 30% probability thermal ellipsoids and labels for non-hydrogen atoms. The atom-labeling scheme has been modified to readily distinguish those atoms that are symmetry related. Symmetry equivalents: O(3) (x, 0.75 − y, 0.75 − z); N(1) (0.75 − x, 0.75 − y, z); O(1) (x, 1.25 − y, 0.25 − z); O(2) (x, 1.25 − y, 0.25 − z); C(2) (0.75 − x, y, 0.75 − z).

$[Cu_2L1(ClO_4)_2]$ (1). H_2L1 (0.41 g, 1.0 mmol) dissolved in methanol (10 mL) was added to an aqueous (10 mL) solution of NaOH (0.080 g, 2.0 mmol). $Cu(ClO_4)_2 \cdot 6H_2O$ (0.74 g, 2.0 mmol) dissolved in water (10 mL) was added and the resulting mixture refluxed for 3 h. Deep blue crystals formed on standing at room temperature, which were collected and recrystallized from acetonitrile/triethyl orthoformate (yield 80%). Anal. Calcd for $Cu_2C_{24}H_{34}N_4O_{10}Cl_2$: C, 39.12; H, 4.65; N, 7.60. Found: C, 38.84; H, 4.42; N, 7.51.

Results and Discussion

Description of the Structure of 1. The crystal structure of **1** is shown in Figure 2 and consists of two copper(II) centers bridged by two phenoxide oxygen atoms with two secondary amine nitrogen donors completing the distorted CuN_2O_2 plane. Interatomic distances and angles relevant to the copper coordination spheres are listed in Table III. Relatively short Cu–O (1.915 (3) Å) and Cu–N (1.986 (5) Å) separations exist in the CuN_2O_2 planes, while long perturbations (Cu–O, 2.821 (3) Å) involving bidentate bridging perchlorates probably best describe the copper coordination spheres as severely distorted, axially elongated, octahedra. The equatorial CuN_2O_2 chromophore is twisted with N(1)–Cu(1)–O(3) angles of 166.9 (2)° and a compressed O(3)–Cu(1)–O(3) angle of 77.2(1)°, and the copper center lies in the mean plane of the N_2O_2 donor set. The two copper atoms are separated by 2.993 (2) Å, with a Cu–O(3)–Cu bridge angle of 102.8 (2)°.

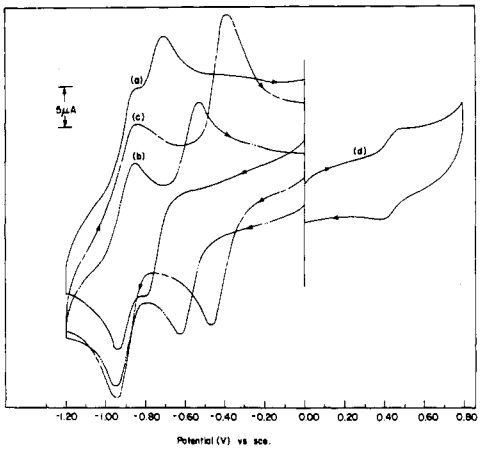

Figure 3. Cyclic voltammograms for (a) $[Cu_2L1(ClO_4)_2]$ (**1**), (b) $[Cu_2L2](ClO_4)_2 \cdot 2H_2O$ (**2**), (c) $[Cu_2L3](ClO_4)_2 \cdot 2H_2O$ (**3**), and (d) ferrocene (GC/Me_2SO/SCE/TEAP).

This structure can be compared with that of the complex $[Cu_2L3Cl_2] \cdot 6H_2O$, involving square-pyramidal copper(II) centers and in-plane Cu–N distances (1.978 Å) slightly shorter and in-plane Cu–O distances (1.981 Å) longer than those in **1**,[7] and also the structure of the mixed-valence-state species $[Cu^{II}Cu^{I}L3]ClO_4 \cdot 0.5CH_3OH$, in which the binuclear cation is essentially planar with Cu–N and Cu–O separations of 1.98 and 1.96 Å, respectively, at the square-planar copper(II) center.[16] The ligand in **1** displays a propeller-like twist, which can be associated with the saturated nitrogen donor centers. In a related system, $[Cu_2L1(CH_3OH)_2](ClO_4)_2$, prepared in dry methanol, the two distorted square-pyramidal copper(II) centers involve axial bonding in a trans arrangement to two coordinated methanol molecules (Cu–O = 2.413 Å). The copper–copper separation (3.088 Å), the Cu–O–Cu bridge angles (103.9°), and Cu–N distances (1.989, 1.991 Å) are comparable with those in **1**, while the Cu–O(phenoxide) distance (1.963 Å) is somewhat longer.[17]

Magnetic, Spectral, and Electrochemical Properties. Compound **1** has a very low room-temperature magnetic moment (μ_{eff} = 0.58 μ_B), less than those observed for **2** (0.71 μ_B)[12a] and **3** (0.72 μ_B),[11] indicating strong antiferromagnetic exchange between the copper(II) centers. In a recent report it has been demonstrated that reasonable estimates of exchange integrals can be obtained from room-temperature effective magnetic moments for binuclear copper(II) complexes by suitable substitution into the Van Vleck exchange equation.[18] Assuming a reasonable value of g (2.1) for **1** at 298 K, a calculated value of 740 cm^{-1} is obtained for $-2J$. Variable-temperature magnetic studies on $[Cu_2L3Cl_2] \cdot 6H_2O$ gave $-2J$ = 588 cm^{-1} with μ_{eff}(285 K) = 0.8 μ_B.[19] Assuming g = 2.1, the calculated value at 285 K for μ_{eff} = 0.8 μ_B is 570 cm^{-1}.[17] The $-2J$ values calculated by the same method (298 K) for **2** and **3** are 650 and 645 cm^{-1}, respectively.

Electronic absorption spectra of **1** in both solid state (mull transmittance; λ_m 360, 580 nm) and solution (MeCN; λ_m (ϵ, L mol^{-1} cm^{-1}) 340 (3648), 580 (282) nm) are almost identical, indicating similar chromophores in both physical states, and also bear a close resemblance to those reported for **2** and **3**. It is of interest to note that as the degree of ligand saturation increases the intensity of the charge-transfer transition in the UV region decreases while that of the visible absorption increases.

Infrared spectra (Nujol mull) of the three compounds are diagnostic in regions associated with NH stretch and Cl–O (ν_3, ClO_4) stretch. For **3** no vibration associated with NH stretch is

(16) Gagné, R. R.; Henling, L. M.; Kistenmacher, T. J. *Inorg. Chem.* **1980**, *19*, 1226.
(17) Charland, J.-P.; Gabe, E. J.; Mandal, S. K.; Thompson, L. K.; Nag, K., unpublished results.
(18) Thompson, L. K.; Ramaswamy, B. S. *Inorg. Chem.* **1986**, *25*, 2664.
(19) Lambert, S. L.; Hendrickson, D. N. *Inorg. Chem.* **1979**, *18*, 2683.

Table IV. Electrochemical Data for Reduction and Oxidation of **1**, **2**, and **3**

complex	Cu^{II}/Cu^{II} ΔE_p,[a] mV	Cu^{II}/Cu^{I} $E_{1/2}$,[b] V	Cu^{II}/Cu^{I} ΔE_p,[a] mV	Cu^{I}/Cu^{I} $E_{1/2}$,[b] V	ΔE,[c] V	K_{con}
$[Cu_2L1(ClO4)_2]$	100[d]	−0.76	100[d]	−0.90	0.14	2.3×10^2
$[Cu_2L2](ClO4)_2 \cdot 2H_2O$	90[d]	−0.58	90[d]	−0.90	0.32	2.6×10^5
$[Cu_2L3](ClO4)_2 \cdot 2H_2O$	90[d]	−0.43	110[d]	−0.90	0.47	9.0×10^7
complex	Cu^{II}/Cu^{II} ΔE_p,[a] mV	Cu^{II}/Cu^{III} $E_{1/2}$,[b] V	Cu^{II}/Cu^{III} ΔE_p,[a] mV	Cu^{III}/Cu^{III} $E_{1/2}$,[b] V	ΔE,[c] V	K_{con}
$[Cu_2L1(ClO4)_2]$	106[e]	1.19	100[e]	1.41	0.22	5.2×10^3[f]
$[Cu_2L2](ClO4)_2 \cdot 2H_2O$	80[e]	1.34				

[a] $\Delta E_p = E_{p,c} - E_{p,a}$ at scan rate 200 mV s^{-1}. [b] $E_{1/2} = 0.5(E_{p,c} + E_{p,a})$ at scan rate 200 mV s^{-1}. [c] $\Delta E = E_{1/2}(\mathbf{1}) - E_{1/2}(\mathbf{2})$. [d] Quasi-reversible. [e] Reversible (ΔE_p invariant as a function of scan rate). [f] $K_{con} = [Cu^{II}Cu^{III}L]^2/([Cu^{II}Cu^{II}L][Cu^{III}Cu^{III}L])$.

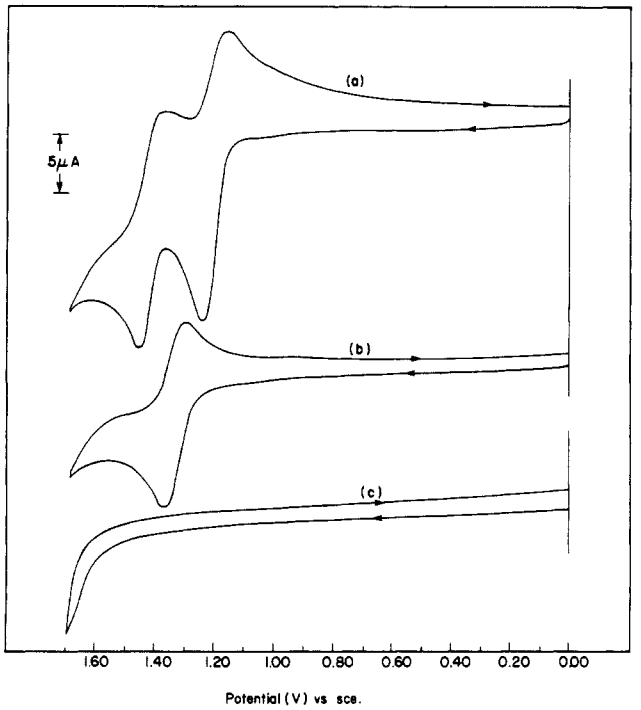

Figure 4. Cyclic voltammograms for (a) $[Cu_2L1(ClO_4)_2]$ (**1**), (b) $[Cu_2L2](ClO_4)_2 \cdot 2H_2O$ (**2**), and (c) $[Cu_2L3](ClO_4)_2 \cdot 2H_2O$ (**3**) (Pt/CH_3CN/SCE/TEAP).

observed, while for **2** a weak band is observed at 3240 cm^{-1} and for **1** a medium-intensity band appears at 3250 cm^{-1}. Compound **3** is characterized by an intense perchlorate absorption at 1100 cm^{-1}, indicative of ionic perchlorate (shoulders at 1120 and 1075 cm^{-1} suggest lower symmetry crystal lattice effects), while for **2** a broad absorption at 1085 cm^{-1} suggests ionic perchlorate also. Three absorptions (1120, 1085, 1025 cm^{-1}) are observed for **1** suggesting a low-symmetry perchlorate group in agreement with the X-ray structural data.

Cyclic voltammograms for the stepwise reduction of compounds **1**–**3** in Me_2SO (glassy-carbon electrode) are shown in Figure 3, while Figure 4 displays cyclic voltammograms for the oxidation of these compounds in CH_3CN (platinum electrode). Electrochemical data for these systems are given in Table IV. H_2L1 shows no electrochemical response in the range +1.7 to −1.2 V. At negative potentials two reduction waves are observed for all compounds. Controlled-potential electrolysis indicates that each wave corresponds to a one-electron reduction step. A dramatic negative shift in the first one-electron reduction potential ($E_{1/2}$ = −0.43 V (**3**), −0.58 V (**2**), −0.76 V (**1**)) is observed as a function of stepwise saturation of the azomethine linkages ($H_2L3 \rightarrow H_2L2 \rightarrow H_2L1$), indicating enhanced stability of the copper(I) state with increased unsaturation. This effect has been observed previously for macrocyclic (N_4), mononuclear copper(II)[20] and nickel(II)[21]

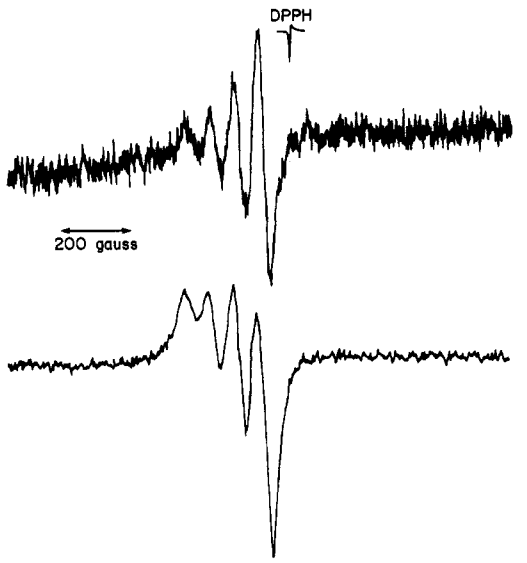

Figure 5. Solution X-band EPR spectra (25 °C) for **1** (one-electron oxidation in CH_3CN (top)) and **2** (one-electron reduction in CH_3CN (bottom)).

complexes but not, to our knowledge, for spin-coupled binuclear systems. A second redox wave, associated with the reduction of the mixed-valence species, is observed for all three compounds at the same potential ($E_{1/2}$ = −0.90 V), independent of the degree of ligand saturation.

The stability of the mixed-valence (Cu(II)–Cu(I)) species increases with increasing ligand unsaturation and can be expressed in terms of the conproportionation constant, K_{con}, where $\Delta E = [E_{1/2}(\mathbf{1}) - E_{1/2}(\mathbf{2})]$.[11]

$$K_{con} = \frac{[Cu^{II}Cu^{I}L]^2}{[Cu^{II}Cu^{II}L][Cu^{I}Cu^{I}L]} = \exp(nF(\Delta E)/RT)$$

The larger the separation between the potentials of the couple, the greater the stability of the mixed-valence species with respect to conproportionation. The values of ΔE and K_{con} are listed in Table IV.

A related trend is observed for the oxidation of **1**–**3** in acetonitrile. No redox waves are observed for **3** in the range 0–1.7 V, while for **2** a single reversible wave ($E_{1/2}$ = 1.34 V) is observed and for **1** two reversible waves ($E_{1/2}$ = 1.19, 1.41 V) are observed (Figure 4) (Table IV). Controlled-potential electrolysis measurements confirm the formation of the species $[Cu^{III}–Cu^{II}L1]^{3+}$ and $[Cu^{III}–Cu^{II}L2]^{3+}$ in acetonitrile by one-electron oxidation of **1** and **2**, respectively. The formation of $[Cu^{III}–Cu^{III}L1]^{4+}$ could not be confirmed by coulometry, but current height measurements indicate that the second oxidation wave for **1** is associated with one-electron transfer. For the mixed-valence-state species K_{con} is 5.2×10^3. Solution EPR spectra at room temperature for the one-electron oxidation (CH_3CN, Figure 5) and one-electron re-

(20) Olson, D. C.; Vasilevskis, J. *Inorg. Chem.* **1971**, *10*, 463.

(21) Lovecchio, F. V.; Gore, E. S.; Busch, D. H. *J. Am. Chem. Soc.* **1974**, *96*, 3109.

duction (Me_2SO) of **1** exhibit four hyperfine lines, consistent with the interaction of the odd electron with just one copper center ($I = {}^3/_2$). In the case of the oxidized species, the copper(III) centers would appear to be low spin. Compound **2** exhibits a clearly resolved four-line spectrum at room temperature on one-electron reduction (CH_3CN, Figure 5) and a poorly resolved four-line spectrum (CH_3CN) on one-electron oxidation. Again, in both cases, the odd electron is localized on one copper center. This behavior contrasts with that of **3**, where at room temperature (CH_2Cl_2 or CH_3CN) seven-line EPR spectra are obtained for the one-electron-reduced species, indicative of interaction of the odd electron with both copper centers.[22]

Oxidation of mononuclear copper(II) species to copper(III),[20,23] the one-electron oxidation of a trinuclear copper(II) system,[24] and the oxidation of a noncoupled binuclear copper(II) system by two one-electron steps[25] have been reported. However, complex **1** represents the first example of a magnetically coupled macrocyclic binuclear copper(II) system that involves two successive one-electron oxidation steps to produce Cu(II)–Cu(III) and Cu(III)–Cu(III) species as well as successive one-electron reduction steps to produce mixed-valence Cu(II)–Cu(I) species and binuclear Cu(I) species.

Acknowledgment. We thank the Natural Sciences and Engineering Research Council of Canada (S.K.M., L.K.T.) and the CSIR, India (K.N.), for financial support for this study and Dr. A. B. P. Lever, York University, for the use of EPR and electrochemistry facilities.

Supplementary Material Available: Listings of anisotropic thermal parameters for **1** (Table SI) and bond lengths and bond angles pertaining to the ligands in **1** (Table SIII) (2 pages); a table of observed and calculated structure factors for **1** (Table SII) (15 pages). Ordering information is given on any current masthead page.

(22) Gagné, R. R.; Koval, C. A.; Smith, T. J. *J. Am. Chem. Soc.* **1977**, *99*, 8367.
(23) Newbecker, T. A.; Kirksey, S. T.; Chellappa, T. K. L.; Margerum, D. W. *Inorg. Chem.* **1979**, *18*, 444.
(24) Datta, D.; Chakravorty, A. *Inorg. Chem.* **1983**, *22*, 1611.
(25) Zacharias, P. S.; Ramachandraiah, A. *Polyhedron.* **1985**, *4*, 1013.

Contribution from the Laboratory of Inorganic Chemistry, University of Thessaloniki, Thessaloniki, Greece, and Department of Chemistry, University of Michigan, Ann Arbor, Michigan 48109

Synthesis and Characterization of Sulfonylurea Complexes with Cd^{2+}, Hg^{2+}, and Ag^+. Crystal and Molecular Structures of K[Cd(chlorpropamide)$_3$] and Hg(tolbutamide)$_2$

D. P. Kessissoglou,*† G. E. Manoussakis,† A. G. Hatzidimitriou,† and M. G. Kanatzidis*‡

Received November 7, 1985

The synthesis and characterization of Cd^{2+}, Ag^+, and Hg^{2+} complexes with deprotonated tolbutamide and chlorpropamide ligands is described. The crystal and molecular structures of $Hg(CH_3C_6H_4SO_2NCONH\text{-}n\text{-}Bu)_2$ (I) and $K[Cd(ClC_6H_4SO_2NCONH\text{-}n\text{-}Pr)_3]$ (III) are reported. In I the coordination environment around the Hg^{2+} atom is strictly linear and the sulfonylurea ligand is bound in a predominantly monodentate fashion. The tolbutamide ligand is bound through the deprotonated sulfamido nitrogen atom. The Hg–N distance is 2.052 (17) Å. By comparison the chlorpropamide ligand is coordinated to a Cd^{2+} atom in a bidentate mode with both the sulfamido nitrogen and the carbonyl oxygen atoms bound to the metal center. The coordination environment around the Cd^{2+} atom can be best described as trigonal prismatic. The mean Cd–N and Cd–O distances are 2.212 (20) and 2.535 (24) Å, respectively. The counterion K^+ slightly interacts with the oxygen of the carbonyl and sulfonyl groups in the anion in such a way as to form a polymeric zigzag K···Cd chain parallel to the *a* axis. The IR spectra show (C⇀O) and (C⇀N) stretching frequencies, characteristic for either mode of sulfonylurea ligand coordination. On the basis of the IR spectra we propose a structure for $K[Ag(p\text{-}XC_6H_4SO_2NCONHR)_2]$ (tolbutamide, X = CH_3 and R = *n*-Bu; chlorpropamide, X = Cl and R = *n*-Pr) similar to that of the Hg^{2+} complexes. The ^1H NMR spectra of these compounds are also reported.

Introduction

Interest in the sulfonylurea class of compounds arises primarily from their ability to reduce blood sugar levels without affecting glucose tolerance.[1] Currently in the United States three sulfonylureas[2] are in use clinically for the management of maturity-onset or stable diabetes. These are *N*-((butylamino)carbonyl)-4-methylbenzenesulfonamide (tolbutamide, A), *N*-((propylamino)carbonyl)-4-chlorobenzenesulfonamide (chlorpropamide, B), and *N*-((cyclohexylamino)carbonyl)-4-acetylbenzenesulfonamide (acetohexamide, C). In addition to these, hundreds of (arylsulfonyl)ureas and related compounds have been synthesized and tested for hypoglycemic activity. The principal mechanism of the hypoglycemic action of the sulfonylureas is stimulation of insulin release by the β-cells of the pancreas.[3a] Generally these drugs induce increase in the insulin levels. In some cases however decrease has been observed.[3b,c] A divalent metal, Zn^{2+}, has been implicated in the release mechanism of insulin and has been found to occur in increased levels in the pancreas. The details of either sulfonylurea drug action and Zn^{2+} involvement or a possible mechanistic relationship between the two in insulin release remain unknown. Furthermore, there has been interest recently in whether

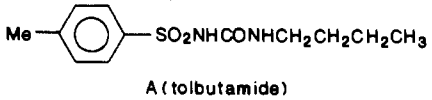

A (tolbutamide)

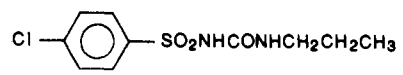

B (chlorpropamide)

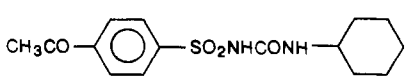

C (acetohexamide)

† University of Thessaloniki.
‡ University of Michigan.

(1) (a) Haack, E. *Arzneim.-Forsch.* **1958**, *8*, 444. (b) Rusvhig, H.; Korger, G.; Aumüller, W.; Wagner, H.; Weyer, R. *Arzneim.-Forsch.* **1958**, *8*, 448. (c) Ruschig, H.; Korger, G.; Aumüller, W.; Wagner, H.; Weyer, R. *Med. Chem.* (*Leverkusen, Ger.*) **1958**, *6*, 61. (d) Gandhi, T. P.; Jindal, M. N. *Arzneim.-Forsch.* **1971**, *21*, 961. Gandhi, T. P.; Jindal, M. N. *Arzneim.-Forsch.* **1971**, *21*, 968.
(2) A related compound is also used: 1-(hexahydro-1*H*-azepin-1-yl)-3-(*p*-toluenesulfonyl)urea (tolazamide)

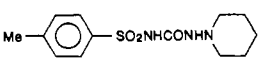

This compound although usually classed as a sulfonylurea is actually a sulfonylsemicarbazide.
(3) (a) Maske, H. *Diabetes* **1957**, *6*, 335. (b) Achelis, J. D.; Hardebeck, K. *Dtsch. Med. Wochenschr.* **1955**, *80*, 1452. (c) Schölz, J.; Bander, A. *Dtsch. Med. Wchenschr.* **1956**, *81*, 825.

0020-1669/87/1326-1395$01.50/0